NOTE / NOTE

A simplified method for 3D slope stability analysis

Zuyu Chen, Hongliang Mi, Faming Zhang, and Xiaogang Wang

Abstract: This paper presents a simplified three-dimensional (3D) slope stability analysis method based on the limit equilibrium theory. The assumption involved in this method is of a parallel intercolumn force inclination, similar to Spencer's method in the two-dimensional (2D) area. It allows for the satisfaction of complete overall force equilibrium conditions and the moment equilibrium requirement about the main axis of rotation. The method has been proven to be numerically tractable for many practical problems. By combining this method with the 3D upper bound approaches, it is possible to bracket the accurate solution of a 3D slope stability analysis problem into a small range.

Key words: slope stability analysis, three-dimensional analysis, limit equilibrium method, upper bound method.

Résumé : Cet article présente un méthode simplifiée d'analyse à 3D de stabilité de talus basée sur la théorie d'équilibre limite. L'hypothèse impliquée dans cette méthode est l'inclinaison parallèle des forces inter tranches, comme dans la zone à 2D de la méthode Spencer. Elle permet de satisfaire complètement les conditions d'équilibre des forces globales et l'exigence de l'équilibre des moments autour de l'axe principal de rotation. On a démontré que la méthode est numériquement soluble pour plusieurs problèmes pratiques. En combinant cette méthode avec des approches de limite supérieure 3D, il est possible de confiner à l'intérieur d'une faible plage la solution précise de l'analyse 3D d'un problème de stabilité de talus.

Mots clés : analyse de stabilité de talus, analyse tridimensionnelle, méthode d'équilibre limite, méthode de limite supérieure.

[Traduit par la Rédaction]

Introduction

Field observations of landslide failure surfaces typically display spatial variability. However, analyses of these slides are usually limited to two-dimensional (2D) approximations. The demand for practical, three-dimensional (3D) slope stability analysis methods and their associated user-friendly computer programs is high (Seed et al. 1990; Morgenstern 1992; Stark and Eid 1998).

There are a large number of publications that deal with 3D slope stability analysis. Duncan (1996) summarized the main aspects of 24 publications dealing with limit equilibrium approaches. This list could now be extended to include recent publications (e.g., Huang and Tsai 2000). All of these methods divide the failure mass into a number of columns with vertical interfaces and use the conditions for static equilibrium to find the factor of safety. Assumptions must be introduced to render the problem statically determinate and to facilitate the numerical procedures. A number of the methods (Hungr et al. 1989; Huang and Tsai 2000) neglect the vertical shear force components of the intercolumn force and project the forces applied on a column in the vertical direction. The normal force of the column base can then be readily determined without the knowledge of the unknown intercolumn forces. Force or moment equilibrium equations are subsequently established to calculate the factor of safety. This kind of treatment can be traced back to 2D analysis, where Bishop (1955) established his simplified method for circular slip surfaces (although complete satisfaction of force equilibrium conditions for an individual slice or for the whole failure mass were not considered). Hungr et al. (1989) discussed the limitations involved in their 3D Bishop and simplified Janbu methods. These do not satisfy the overall force equilibrium condition in the lateral direction. Huang and Tsai (2000) employ moment equilibrium conditions around two co-ordinate axes. However, since the force equilibrium equations are not fully satisfied in their method, the moment equilibrium conditions are dependent upon the location of the axes around which the moments are calculated. Their method is therefore only applicable to spherical slip surfaces in which the location of the center is known and allows the establishment of the moment equilibrium condi-

Received 22 August 2001. Accepted 1 November 2002. Published on the NRC Research Press Web site at http://cgj.nrc.ca on 22 May 2003.

Z. Chen[1] and X. Wang. China Institute of Water Resources and Hydropower Research, P.O. Box 366, 20 West Chegongzhuang Road, Beijing, 100044, China (PRC).
H. Mi. Department of Hydraulic Engineering, Tsinghua University, Beijing, 100084, China (PRC).
F. Zhang. Department of Geology, Hehai University, Nanjing, 210024.

[1]Corresponding author (e-mail: chenzy@tsinghua.edu.cn).

 doi: 10.1139/T03-002

tions. Our profession accepts these simplifications on the basis that they have be validated through practical application and more rigorous methods.

Lam and Fredlund (1993) established a 3D method based on the complete satisfaction of force equilibrium conditions for each column. Their governing equations of force and moment equilibrium for the whole failure mass involve a large number of unknown intercolumn forces. Convergence issues can be of concern as essentially "trial and error" numerical procedures are used to solve these large-scale, nonlinear equations.

Table 1 summarizes the assumptions involved in some representative 3D methods.

As a complimentary approach, a 3D stability analysis based on the upper bound theorem of plasticity has been developed (Michalowski 1980; Chen et al. 2001*a*, *b*). It is theoretically more rigorous than various simplified limit equilibrium methods. However, it includes a procedure for finding the critical failure mode that is composed of a slip surface and a series of inclined interfaces of blocks or columns. The numerical optimization algorithm involves a large number of degrees of freedom, resulting in a challenging mathematical endeavor. Solutions higher than the accurate values may occasionally be obtained if the numerical procedure terminates prematurely. The limit equilibrium methods, which approach the accurate solution from the lower bound (Chen 1999), can be coupled with the upper bound methods and hopefully, bracket the solution into a small range.

This paper presents a simplified 3D limit equilibrium method based on the assumption of parallel intercolumn forces on row-interfaces, an approach that has been widely accepted in the 2D area (Spencer 1967). This 3D method renders more satisfied equilibrium equations and freedom in the shape of the slip surface. It requires relatively simple numerical procedures (with demonstrated high efficiency) to obtain convergence. The computation results using this method are justified by other simplified approaches as well as the 3D upper bound method proposed by Chen et al. (2001*a*, *b*).

The proposed 3D limit equilibrium method

Assumptions made for the internal shear forces on a column

As with other 3D limit equilibrium methods, the failure mass is divided into a number of columns with vertical interfaces (Fig. 1). The conventional definition for factor of safety F reduces the available shear strength parameters c' and ϕ' by the following equations to bring the slope to a limiting state.

$$[1] \qquad c'_e = \frac{c'}{F}$$

$$[2] \qquad \tan\phi'_e = \frac{\tan\phi'}{F}$$

Throughout this paper, the subscript "e" is used to indicate the variables that are determined based on the reduced shear strength parameters c'_e and ϕ'_e.

The following assumptions are made in the establishment of the force and moment equilibrium equations (Fig. 2).

Table 1. Assumptions involved in various 3D slope stability analysis methods.

	Assumptions made on the components of the internal shear forces					Satisfaction of the overall force equilibrium conditions in the three co-ordinate axes			Satisfaction of the overall moment equilibrium conditions around the three co-ordinate axes			
		On the row-interface		On the column-interface								
Authors	On the column base in z-axis	In y-axis	In z-axis	In x-axis	In y-axis	x	y	z	x	y	z	Shape of the slip surface
Hungr (1989) (Bishop)	Neg.	Neg.	Neg.	Neg.	Neg.	No	Yes	No	No	No	Yes	Spherical and symmetrical
Hungr (1989) (Janbu)	Neg.	Neg.	Neg.	Neg.	Neg.	Yes	Yes	No	No	No	No	Symmetrical
Zhang (1988)	Neg.	(A constant value of inclination for the resultant of all intercolumn forces)				Yes	Yes	No	No	No	Yes	Symmetrical
Chen and Chameau (1983)	Neg.	Inc.	Neg.	(To be parallel to the column base)		Yes	Yes	No	No	No	Yes	Symmetrical
Lam and Fredlund (1993)	Neg.	Inc.	Neg.	Neg.	Inc.	Yes	Yes	Yes	No	No	Yes	Generalized
Huang and Tsai (2000)	Inc.	Neg.	Neg.	Neg.	Neg.	No	Yes	No	Yes	No	Yes	At least partly spherical
This paper	Inc.	Inc.	Neg.	Neg.	Neg.	Yes	Yes	Yes	No	No	Yes	Generalized

Note: Neg., the referred component is neglected in the force and (or) moment equilibrium equations; Inc., means that it is included.

Fig. 1. Discretization of a failure mass.

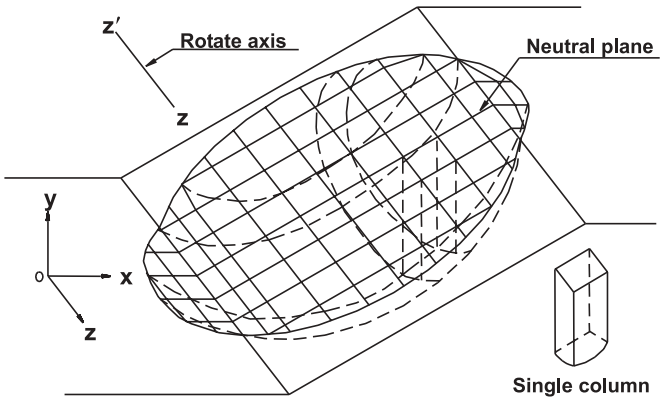

(1) The horizontal shear forces, H, on the row-interfaces (ABFE and DCGH in Fig. 2*a*) are neglected, i.e., the intercolumn forces with inclinations of β to the x-axis and designated G, are assumed to be parallel to the xoy plane. It is further assumed that β is constant for all columns. This treatment is therefore equivalent to that used in Spencer's (1967) method in two dimensions. Ignoring the horizontal components of shear forces on the row-interfaces is a common assumption made to almost all of the 3D methods appearing in the literature (refer to Table 1).

(2) Shear forces, P and V, applied to the column-interfaces (ADHE and BCGF in Fig. 2) are neglected. Similar assumptions have been made by other researchers (e.g., Hungr et al. 1989; Huang and Tsai 2000).

(3) The shear force applied to any column base, T, is assumed to be inclined at an angle of ρ measured from the xoy plane to the positive z-axis. For prisms in any column direction (i.e., those with constant z values), ρ is taken to be constant. In the z-direction, ρ varies according to the following two modes:

(*a*) Mode I: the direction of the shear forces on all of the column bases is the same, i.e., $|\rho| = \kappa$ = constant (Fig. 3*a*).

(*b*) Mode II: the basal shear forces on the left and right side of the central xoy plane take opposite directions and vary linearly with respect to the z-axis, i.e., (Fig. 3*b*),

$$[3]\qquad \begin{aligned} \rho_R &= \kappa z \qquad z \geq 0 \\ \rho_L &= -\eta\kappa z \qquad z < 0 \end{aligned}$$

The subscripts R and L indicate the right and left sides of the xoy plane, respectively, η is a coefficient of asymmetry, and κ is an unknown involved in the force and moment equilibrium equations. It determines the magnitude of ρ for each column after the solution is obtained.

The direction cosines of the shear force T, designated m_x, m_y, m_z, can be readily determined by the following equations:

$$[4]\qquad \begin{cases} m_x^2 + m_y^2 + m_z^2 = 1 \\ m_x n_x + m_y n_y + m_z n_z = 0 \end{cases}$$

and

$$[5]\qquad m_z = \sin\rho$$

where n_x, n_y, n_z are direction cosines of the normal to the column base. There are two solutions to m_x. The negative solution should be rejected.

The force and moment equilibrium equations and their solutions

The procedures for calculating the factor of safety are as follows (refer to Fig. 4).

(1) Determine the normal force N_i applied to each column base

By projecting all of the forces in the direction $\boldsymbol{S}'$ applied to each column (that is perpendicular to the intercolumn forces $\boldsymbol{G}$), it is possible to calculate the normal force N_i applied to each column base. As $\boldsymbol{G}_i$ and $\boldsymbol{G}_{i+1}$, applied on the front and rear row-interfaces, respectively, are assumed to be parallel to the xoy plane and inclined at a constant angle of β, they do not appear in the projection. The shear forces on the column-interfaces (ADHE and BCGF in Fig. 2), which have been assumed to be zero, also do not appear. This results in the following equation which involves only one unknown, the normal force N_i:

$$[6]\qquad \begin{aligned} -W_i\cos\beta + N_i(-n_x\sin\beta + n_y\cos\beta) \\ + T_i(-m_x\sin\beta + m_y\cos\beta) = 0 \end{aligned}$$

The shear force, T_i, on the column base can be determined by application of Mohr–Coloumb's failure criterion

$$[7]\qquad T_i = (N_i - uA_i)\tan\phi_e' + c_e' A_i$$

where u is the pore pressure at the column base (of area A_i) and W_i is the weight of the column. The normal force N_i applied to the column base can be consequently obtained from

$$[8]\qquad N_i = \frac{W_i\cos\beta + (uA_i\tan\phi_e' - c_e' A_i)(-m_x\sin\beta + m_y\cos\beta)}{-n_x\sin\beta + n_y\cos\beta + \tan\phi_e'(-m_x\sin\beta + m_y\cos\beta)}$$

(2) Establish the force equilibrium equation in the other two co-ordinate axes and the moment equilibrium equation about the z-axis

By projecting the forces applied to the entire failure mass in the direction $\boldsymbol{S}$ (i.e., in the $\boldsymbol{G}$ direction), we obtain

$$[9]\qquad \begin{aligned} S = \sum[N_i(n_x\cos\beta + n_y\sin\beta)_i \\ + T_i(m_x\cos\beta + m_y\sin\beta)_i - W_i\sin\beta] = 0 \end{aligned}$$

The overall force equilibrium in the z-direction requires

$$[10]\qquad Z = \sum(N_i\cdot n_z + T_i\cdot m_z) = 0$$

Establishing the overall moment equilibrium equation about the z-axis leads to

$$[11]\qquad \begin{aligned} M = \sum[-W_i x - N_i\cdot n_x\cdot y \\ + N_i\cdot n_y\cdot x - T_i\cdot m_x\cdot y + T_i\cdot m_y\cdot x] = 0 \end{aligned}$$

where x, y, z are co-ordinate values of the center of a column base. Since the force equilibrium conditions for the three

Fig. 2. Forces applied on a prism (*a*) before introducing the assumptions and (*b*) assumptions made for the shear forces on the prism.

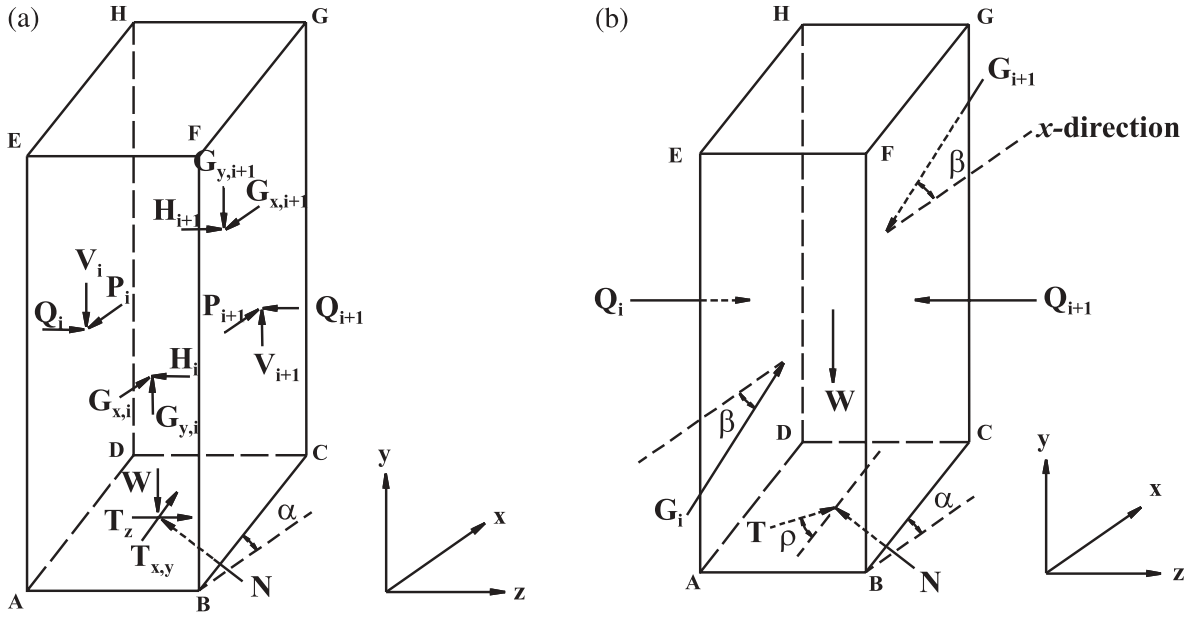

co-ordinate axes are all satisfied, eq. [11] can be established around any arbitrary *z*- axis.

Equations [9], [10], and [11] are controlling equations for solving for the factor of safety. A simple way of justifying these equations is by summing up all of the dot products made by the forces and their projection axis. The direction cosines for the individual vectors are: $(\cos\beta, \sin\beta, 0)$ for $\boldsymbol{S'}$; $(0, -1, 0)$ for $\boldsymbol{W}$; (n_x, n_y, n_z) for $\boldsymbol{N}$; (m_x, m_y, m_z) for $\boldsymbol{T}$; and $(-\sin\beta, \cos\beta, 0)$ for $\boldsymbol{S}$.

(3) Solve for the factor of safety using the Newton–Raphson method

There are three unknowns, namely F, β, and ρ (or k if mode II for the distribution function of ρ is used) involved in eqs. [9], [10], and [11]. They can be obtained by application of the Newton–Raphson method. Assuming a set of initial guesses F_0, β_0, and ρ_0 normally gives nonzero values of ΔS, ΔM, and ΔZ from eqs. [9], [10], and [11]. The next set of the unknowns, represented as F_1, β_1 and ρ_1, will make ΔS, ΔM, and ΔZ closer to zero if they are obtained by the following equations ($i = 0$, at present):

$$[12] \qquad \Delta F = F_{i+1} - F_i = -\frac{K_F}{D}$$

$$[13] \qquad \Delta\beta = \beta_{i+1} - \beta_i = -\frac{K_\beta}{D}$$

$$[14] \qquad \Delta\rho = \rho_{i+1} - \rho_i = -\frac{K_\rho}{D}$$

where

$$[15] \qquad D = \begin{vmatrix} \frac{\partial S}{\partial F} & \frac{\partial S}{\partial \beta} & \frac{\partial S}{\partial \rho} \\ \frac{\partial M}{\partial F} & \frac{\partial M}{\partial \beta} & \frac{\partial M}{\partial \rho} \\ \frac{\partial Z}{\partial F} & \frac{\partial Z}{\partial \beta} & \frac{\partial Z}{\partial \rho} \end{vmatrix}$$

$$[16] \qquad K_F = \begin{vmatrix} \Delta S & \frac{\partial S}{\partial \beta} & \frac{\partial S}{\partial \rho} \\ \Delta M & \frac{\partial M}{\partial \beta} & \frac{\partial M}{\partial \rho} \\ \Delta Z & \frac{\partial Z}{\partial \beta} & \frac{\partial Z}{\partial \rho} \end{vmatrix}$$

$$K_\beta = \begin{vmatrix} \frac{\partial S}{\partial F} & \Delta S & \frac{\partial S}{\partial \rho} \\ \frac{\partial M}{\partial F} & \Delta M & \frac{\partial M}{\partial \rho} \\ \frac{\partial Z}{\partial F} & \Delta Z & \frac{\partial Z}{\partial \rho} \end{vmatrix}$$

$$K_\rho = \begin{vmatrix} \frac{\partial S}{\partial F} & \frac{\partial S}{\partial \beta} & \Delta S \\ \frac{\partial M}{\partial F} & \frac{\partial M}{\partial \beta} & \Delta M \\ \frac{\partial Z}{\partial F} & \frac{\partial Z}{\partial \beta} & \Delta Z \end{vmatrix}$$

The iteration terminates when the absolute values of ΔF, $\Delta\beta$, and $\Delta\rho$ obtained from eqs. [12], [13], and [14] are all less than an allowable limit, usually taken as 0.001 (β and ρ are in radians).

Fig. 3. Assumption made for the distribution of *r*: (*a*) mode I, (*b*) mode II.

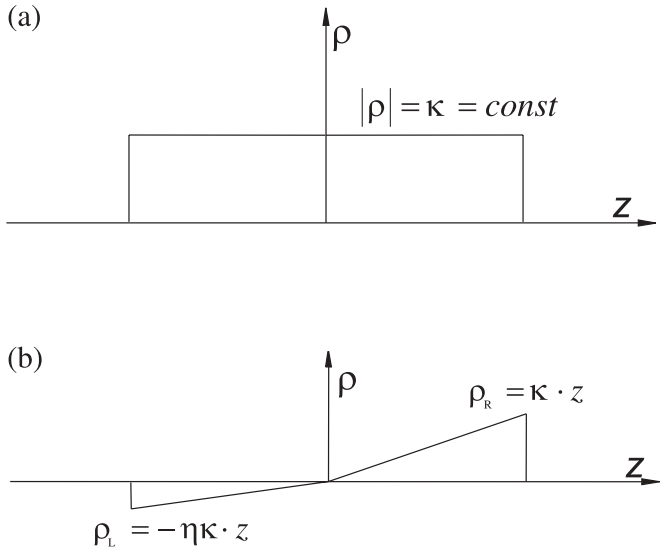

Fig. 4. The force and moment equilibrium on *S′*.

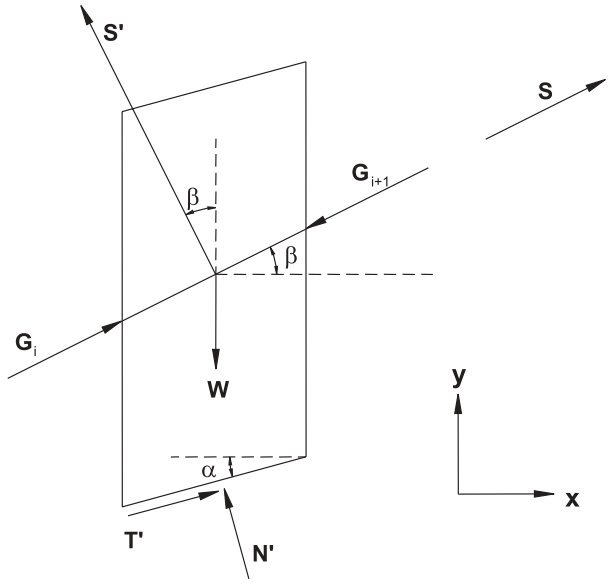

Conditions of physical admissibility

In 2D analysis, the solution associated with a certain mode of assumption for the interslice forces should be subjected to the restriction of physical admissibility (Morgenstern and Price 1965; Chen and Morgenstern 1983). In the 3D analysis, since the intercolumn forces usually are not fully resolved, only the condition where there is no tension on the column bases is imposed, i.e.,

$$[17] \quad N_i - uA_i \geq 0$$

Illustrative examples

Example 1: Zhang's (1988) example problem of an ellipsoidal spherical slip surface

The two example problems presented by Zhang (1988) are shown in Fig. 5. These problems have been re-evaluated by a number of authors as part of the validation process for their new 3D analysis methods (Lam and Fredlund 1993; Huang and Tsai 2000). Chen et al. (2001*a*) used their upper bound method to analyze the circular slip surface at the central *xoy* plane. They obtained a factor of safety of $F = 2.262$. This can be compared to Zhang's solution of $F = 2.122$. Re-analysis using the proposed limit equilibrium method results in $F = 2.187$.

For this symmetrical problem, the slip surface is a circle at the central *xoy* plane, but is ellipsoidal in the *z*-axis direction. Using the mode I distribution function for ρ depicted in Fig. 3*a*, the factor of safety can be obtained using the iteration procedure listed in Table 2. It can be seen that an initial input for *F*, β, and ρ of 2.284, 5.0°, and 5.0°, respectively, results in a converged solution of $F = 2.187$. This is reasonably close to Zhang's solution of $F = 2.122$. The unbalanced forces and moments are seen to decrease rapidly and by the third iteration are close to zero. The solution for ρ is zero, as would be anticipated for a problem with a symmetrical failure surface. A subsequent calculation using the mode II distribution function for ρ (refer to Fig. 3*b*) with $\eta = 1$ gave a solution of $F = 2.188$.

A further example, which includes a plane as part of the slip surface, is shown as case 2 in Fig. 5. This example, from Zhang (1988), has also been re-evaluated by a number of authors. The results obtained by the proposed method, compared to those provided by other researchers are listed in Table 3. The inclination of row interfaces for the critical failure mode, assessed by the upper bound method (Chen et al. 2001), is shown in Fig. 6. The factor of safety of $F = 1.717$ obtained for this critical mode is slightly higher than that obtained by others. However, in general, the factors of safety obtained for this problem using different approaches are in reasonably close agreement. As with the previous example, rapid convergence was obtained using this limit equilibrium method.

As commented on by Lam and Fredlund (1993), the two example cases shown in Fig. 5 are extensions of the 2D examples presented by Fredlund and Krahn (1977). To further validate this 3D method, the plain strain simplifications of cases 1 and 2 have been evaluated. The test examples consist of nine identical cross sections at 10 m spacing. The factors of safety obtained by the plain strain 3D method are 2.108 and 1.384 for cases 1 and 2, respectively, compared with 2.073 and 1.373 obtained by Fredlund and Krahn using Spencer's method. The intercolumn force inclinations, β, obtained from Fredlund and Krahn's 2D and 3D methods were also very similar. For case 1, the values of β for the 2D and 3D analyses were 14.81 and 14.87°, respectively, while for case 2 they were 10.49 and 10.13°, respectively.

Example 2: wedge failure analysis

Stability analyses of wedge failures in rock masses using the limit equilibrium method are illustrated in many reference books (e.g., Hoek and Bray 1977). The limitations of this simplistic approach include the assumption of uniform material properties and the assumed direction of the shear forces (parallel to the line of intersection of the two failure

Fig. 5. Zhang's example, case 1: an ellipsoid sphere slip surface; case 2: the slip surface with a composite shape containing a weak plane.

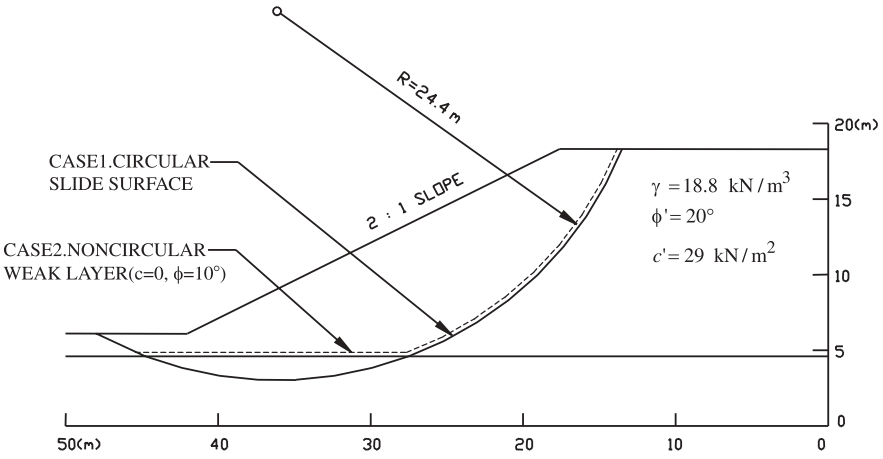

Table 2. The iteration process for Zhang's example, case 1 in Fig. 5.

Iteration	F	β (°)	ρ (°)	Unbalanced force, S (kN)	Unbalanced moment, M (kN·m)	Unbalanced force, Z (kN)
0	2.284	5.0	5.0	–9166.1	98 701.9	6727.4
1	2.164	12.42	–0.25	–391.9	23 620.0	–351.6
2	2.187	14.85	0	12.9	165.0	–2.7
3	2.187	14.87	0	0.5	–0.2	0.3

Table 3. Comparisons of the results from various authors for Zhang's example, case 2 in Fig. 5.

Zhang (1988)	Hungr et al. (1989)	Lam and Fredlund (1993)	Huang and Tsai (2000)	Chen et al. (2001*a*)	Present study
1.553	1.620	1.603	1.658	1.717	1.64

surfaces). The 3D method presented in this paper can be used to analyze more complex wedge failure problems.

Two examples involving simple geometry and material properties have been analyzed using the new 3D method. The parameters defining the problems are listed in Table 4. The parameters have been chosen so that the solution from the 3D method can be compared to those obtained from the traditional approach. Figure 7 shows the symmetric wedge used in the 3D analysis. The 3D analysis resulted in a factor of safety of F = 1.556, which is the same as that obtained from the traditional analysis. For the mode I distribution function of ρ, ρ converged to zero. Taking η as unity and adopting the mode II distribution of ρ also gave a factor of safety of 1.556 and a converged κ in eq. [3] of zero.

Figure 8 depicts an asymmetric wedge; geometric and material parameters are listed in Table 4. A solution could not be achieved using the mode I distribution for ρ. The mode II distribution (using various values for η) resulted in factors of safety (see Table 5) varying from 1.597 to 1.615. Traditional analysis results in F = 1.640. This example shows that by taking different values for η, consistent values of F are obtained, as long as the condition of physical admissibility as specified by eq. [17] is met.

Fig. 6. Zhang's example of case 2, the critical inclination of row-interfaces in the upper bound solution.

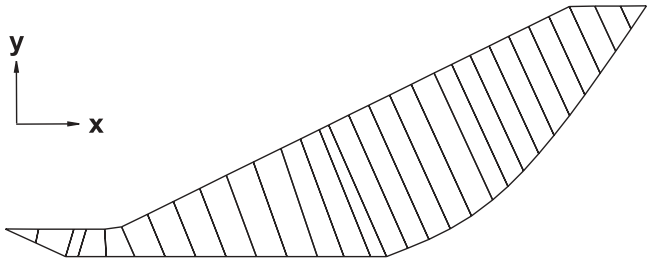

Examples of practical applications

Reinforcement of a high slope within Quaternary deposit

Figure 9 shows a Quaternary deposit "hanging" over an expected reservoir created by the 300 m high Xiao Wan arch dam that is currently being built in Yunnan Province, China. This potentially unstable deposit is 400 m high with a total volume of 5.0 ×10^6 m^3. Excavation of the arch dam foundation will cut away part of the toe of the slope. The high magnitude of seismicity further adds to concerns over long-term

Table 4. Parameters for wedge examples.

	Symmetric example		Asymmetric example	
Planes	Dip (°)	Dip angle (°)	Dip (°)	Dip angle (°)
Left	115	45	120	40
Right	245	45	240	60
Surface	180	10	180	0
Slope	180	60	180	60

Note: Both left and right failure planes take the same shear strength parameters. For the symmetric case, $c' = 0.02$ MPa, $\phi' = 20°$; and for the asymmetric case, $c' = 0.05$ MPa, $\phi' = 30°$.

Fig. 7. Example of a symmetric wedge.

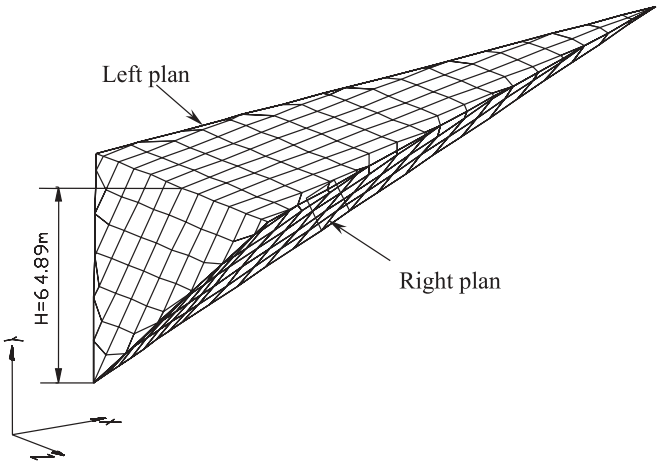

stability. Detailed geological exploration has identified the isometric contour of the deposit–bedrock interface where a thick clay seam was discovered, forming a "spoon shaped" potential slip surface (Fig. 10). In addition to the drainage tunnels to be built in the bedrock, reinforcement work is believed to be necessary. One alternative involves a series of prestressed cables, each 3000 kN in capacity and 180 m in length, which are bounded around the slope to "hold" the soil mass. Both ends of the cables are embedded in the rock of the upstream and downstream gullies (refer to Fig. 9). The aim of the 3D stability analysis is to determine the increase in factor of safety resulting from implementation of the proposed cable layout. This layout involves cables at 1 m spacing, between elevations of 1150 and 1300 m. The supporting forces of the cables can be readily determined by applying the design methods for cable bridges. The calculations resulted in a total load supplied by the cable system of 1.37×10^6 kN in essentially the horizontal direction.

The failure mass is approximated by six cross sections in the pre-excavation case and by five post-excavation. In the post-excavation case, cross section 2 is removed and sections 0 and 1 are partly cut out at the toe (refer to Fig. 9). Comprehensive shear strength parameters of $\phi' = 35°$ and $c' = 0.05$ MPa have been assumed for the slip surface. Although most of the slip surface will coincide with the clay seam at the deposit–bedrock interface, optimization is needed to determine the critical locations of the points defining the interception of the slip surface with the slope surface at the crown and toe. Figure 11 shows the critical slip surface for the excavation case for each cross section obtained through optimization. The interception points are marked by their respective elevations.

Fig. 8. Example of an asymmetric wedge.

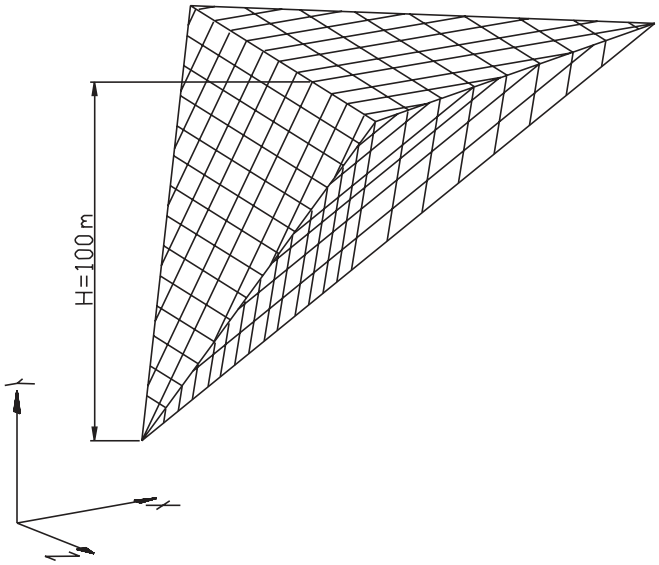

Table 5. Factors of safety associated with different values of η in mode II for the example of an asymmetric wedge.

η	1.2	1.1	1.0	0.9	0.8	0.7	0.6
κ	0.750	0.770	0.795	0.821	0.849	0.880	0.991
F	1.615	1.612	1.611	1.608	1.605	1.601	1.597

Both limit equilibrium and upper bound methods have been used to evaluate the factors of safety. Table 6 shows the results for various operational cases. It was found that for the upper bound calculation, the degrees of freedom numbered as high as 16 if the inclinations of the interfaces between the columns were included. This brought considerable difficulties in finding the global minimum of factor of safety. An approximate approach, where no effort was made to find the critical inclinations of the interfaces, was adopted instead. The interfaces were assumed to be vertical and have relatively low shear strength parameters of $\phi' = 10°$ and $c' = 0.04$ MPa. This approach to some extent, compensates for the higher factor of safety obtained by not optimizing the interface inclinations. The results listed in Table 6 show that excavation of the toe of the Quaternary deposit reduces the factor of safety by 7%. The combination of the various stabilizing measures increases the factors of safety by 15–20% and results in a reduction of about 10% if obtained under earthquake loading.

It was interesting to find that even for this problem, which exhibits marked asymmetry in the shape of the failure mass, there was no substantial difference among the more rigorous 3D methods described in this paper and those obtained using Jambu's simplified 3D method (Hungr et al. 1989). Also worth noting are the factors of safety obtained by the quasi-3D method using the weighted-average approach, which are in most cases lower than the more rigorous 3D methods by 0.10. In this example, this difference means several meganewtons of supporting force that can be saved if the 3D methods are employed.

Fig. 9. The Quaternary deposit of the Xiao Wan Project and the proposed reinforcement by prestressed cables.

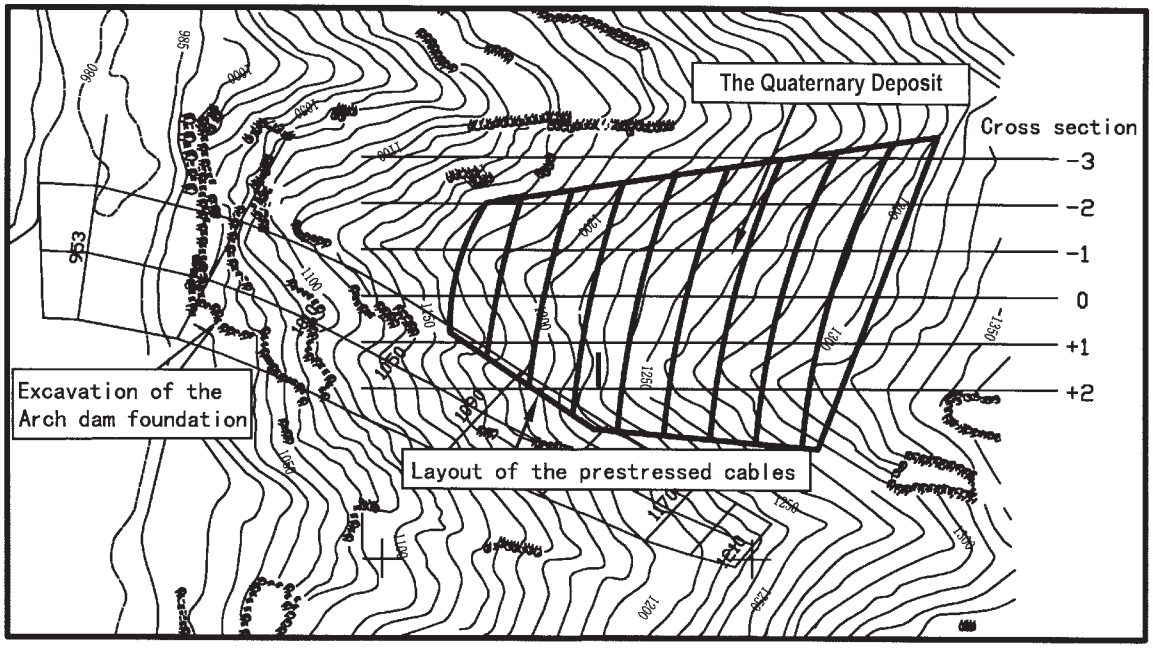

Table 6. Evaluation of factors of safety upon various operational cases.

			FOS by various methods			
No.	Case	r_u	Upper bound (Chen et al. 2001*a*)	Limit equilibrium (this paper)	Weighted average	Simplified Janbu (Hungr et al. 1989)
1	Original topography	0.15	1.154	1.138	1.042	1.089
2	After excavation	0.15	1.087	1.063	1.014	1.02
3	2 + drainage	0.05	1.239	1.216	1.160	1.174
4	3 + reinforcing cables	0.05	1.343	1.357	1.229	1.252
5	4 + earthquake	0.05	1.198	1.180	0.998	1.117

Note: r_u, pore pressure coefficient.

Fig. 10. Sketches for 3D calculations for the high Quaternary deposit after excavation: (*a*) isometric view; (*b*) plan view.

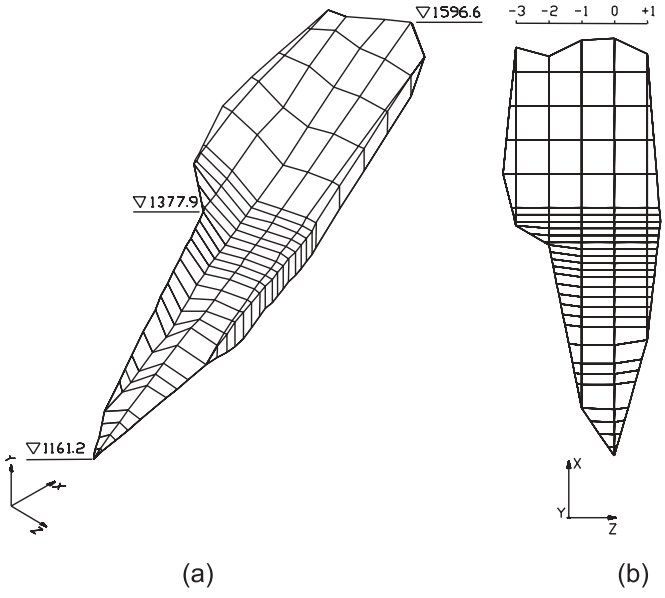

Discussions and concluding remarks

From Table 1 it can be seen that all of the existing limit equilibrium methods, except Lam and Fredlund's, fail to satisfy the force equilibrium condition in the lateral direction (i.e., the *z*-axis). This has resulted in concern over the accuracy of the solution (Hungr et al. 1989) and the limitations to the slip surface, such as symmetrical (Chen and Chameau 1983), partly spherical (Huang and Tsai 2000), or logarithmic (Leshchinsky et al. 1986). The main innovation of the proposed method is the satisfaction of overall force equilibrium conditions in all three directions. This method is therefore most useful for slip surfaces with marked asymmetry in the lateral direction. Although different 3D methods appear to give virtually the same results for the examples shown in this paper, much more practical applications will be needed to fully understand the applicability and limitations of these methods.

Another feature of this method is its simplicity and numerical tractability. Compared to Spencer's 2D method, only one additional equation for equilibrium in the *z*-direction has been added. The Newton–Raphson iteration procedure has enabled very rapid convergence for all of the examples shown in this paper.

Fig. 11. Cross sections of the Quaternary deposit example (refer to Fig. 10).

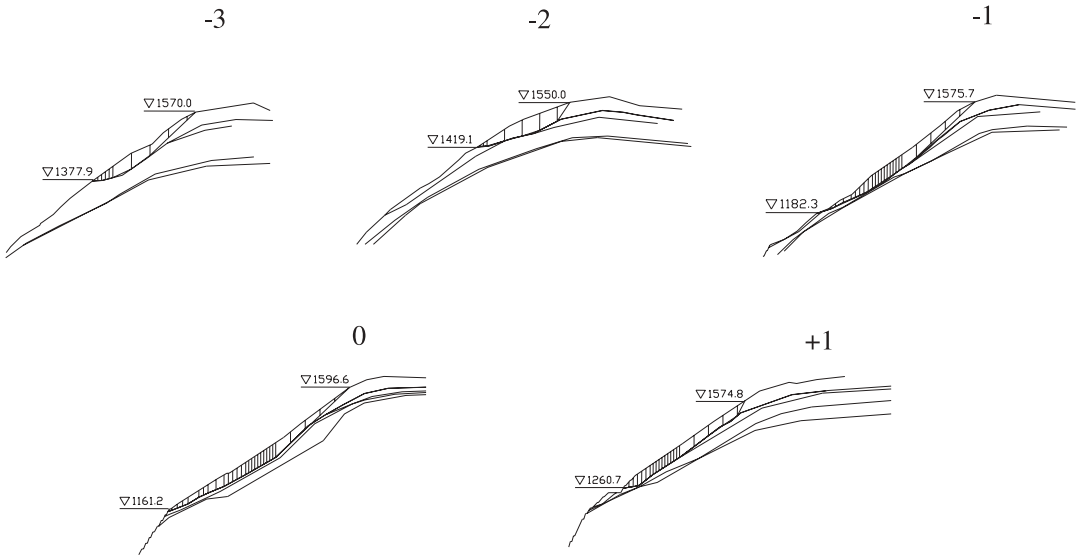

However, the method still represents a simplified approach as the static equilibrium condition is not fully satisfied for each column, and some shear components of the intercolumn forces are neglected. Its usefulness will be justified in its practical applications and by the complimentary use of other more rigorous methods, such as the upper bound method (Michalowski 1980; Chen et al. 2001*a*).

To facilitate the application of this method, source programs in FORTRAN language have been provided in the web site: www.geoeng.iwhr.com/geoeng/download.htm.

Acknowledgement

This work is supported by China National Natural Science Foundation (contract number: 50179039).

References

Bishop, A.W. 1955. The use of the slip circle in the stability analysis of slopes. Géotechnique, **5**(1): 7–17.

Chen, Z. 1999. Keynote lecture: The limit analysis for slopes: Theory, methods, and applications. *In* Proceedings of the International Symposium on Slope Stability Analysis, Mastuyama, Japan, 8–11 November. *Edited by* N. Yagi, T. Yamagami, and J. Jiang. A.A. Balkema, Rotterdam. Vol. 1, pp. 31–48.

Chen, R., and Chameau J.L. 1983. Three-dimensional limit equilibrium analysis of slopes. Géotechnique, **33**: 31–40.

Chen, Z., and Morgenstern, N.R 1983. Extensions to the generalized method of slices for stability analysis. Canadian Geotechnical Journal, **20**: 104–109.

Chen, Z., Wang, X., Haberfield, C., Yin, J., and Wang, Y. 2001*a*. A three-dimensional slope stability analysis method using the upper bound theorem, Part I: Theory and methods. International Journal of Rock Mechanics and Mining Sciences, **38**: 369–378.

Chen, Z., Wang, J., Yin, J., Wang, Y., and Haberfield, C. 2001*b*. A three-dimensional slope stability analysis method using the upper bound theorem, Part II: Numerical approaches, applications and extensions. International Journal of Rock Mechanics and Mining Sciences, **38**: 379–397.

Duncan J.M. 1996. State of the art: Limit equilibrium and finite element analysis of slopes. Journal of Geotechnical Engineering. ASCE, **122**(7): 577–596.

Fredlund, D.G., and Krahn, J. 1977. Comparison of slope stability analysis. Canadian Geotechnical Journal, **14**: 429–439.

Hoek, E., and Bray J.W. 1977. Rock slope engineering. The Institution of Mining and Metallurgy, London.

Huang, C.C., and Tsai, C.C. 2000. New method for 3D and asymmetric slope stability analysis. Journal of Geotechnical and Environmental Engineering, ASCE, **126**(10): 917–927.

Hungr, O., Salgado, F.M and Byrne, P.M. 1989. Evaluation of a three-dimensional method of slope stability analysis. Canadian Geotechnical Journal, **26**: 679–686.

Lam, L., and Fredlund, D.G. 1993. A general limit-equilibrium model for three-dimensional slope stability analysis. Canadian Geotechnical Journal, **30**: 905–919.

Leshchinsky, D., and Baker, R. 1986. Three dimensional analysis of slope stability. Soils and Foundations, **26**(4): 98–110.

Michalowski, R.L. 1980. Three-dimensional analysis of locally loaded slopes. Géotechnique, **39**: 27–38.

Morgenstern, N.R. 1992. The evaluation of slope stability – A 25 year perspective. *In* Proceedings of the ASCE Speciality Conference on Stability and Performance of Slopes and Embankments II, University of California, Berkeley, 29 June – 1 July. pp. 1–26.

Morgenstern, N.R., and Price, V. 1965. The analysis of the stability of general slip surface. Géotechnique, **15**(l): 79–93.

Seed, R.B, Mitchell, J.K., and Seed, H.B. 1990. Kettlemen Hills waste landfill slope failure, II: stability analysis. Journal of Geotechnical Engineering, ASCE, **116**(4): 669–690.

Spencer, E. 1967. A method of analysis of stability of embankments assuming parallel inter-slice forces. Géotechnique, **171**: 11–26.

Stark, T.D., and Eid, H.T. 1998. Performance of three-dimensional slope stability analysis method in practice. Journal of Geotechnical Engineering, ASCE, **124**: 1049–1060.

Zhang, X. 1988. Three-dimensional stability analysis of concave slopes in plan view. Journal of Geotechnical Engineering, ASCE, **114**: 658–671.